
MORPHOLOGY-BASED NON-RIGID REGISTRATION OF CORONARY COMPUTED TOMOGRAPHY AND INTRAVASCULAR IMAGES THROUGH VIRTUAL CATHETER PATH OPTIMIZATION

 **Karim Kadry***

Institute of Medical Engineering and Science
Massachusetts Institute of Technology
Cambridge, MA 02139
kkadry@mit.edu

Abhishek Karmakar

Meinig School of Biomedical Engineering
Cornell University
Ithaca, NY 14850
ak944@cornell.edu

Andreas Schuh

Biomedical Image Analysis Group
Imperial College London
HeartFlow, Inc., USA
London, UK
aschuh@heartflow.com

Kersten Peterson

HeartFlow, Inc., USA
Redwood City, CA, 94063, USA
kpetersen@heartflow.com

Michiel Schaap

HeartFlow, Inc., USA
Redwood City, CA, 94063, USA
mschaap@heartflow.com

David Marlevi

Department of Molecular Medicine and Surgery
Karolinska Institute
Stockholm, Sweden
david.marlevi@ki.se

Charles Taylor

Department of Electrical Engineering
HeartFlow, Inc., USA
Redwood City, CA, 94063, USA
ctaylor@heartflow.com

Elazer Edelman

Institute of Medical Engineering and Science
Massachusetts Institute of Technology
Cambridge, MA 02139
ere@mit.edu

Farhad Nezami

Department of Surgery
Brigham and Women's Hospital Harvard Medical School
Boston, MA 02115
frikhtegarnezami@bwh.harvard.edu

ABSTRACT

Coronary Computed Tomography Angiography (CCTA) provides information on the presence, extent, and severity of obstructive coronary artery disease. Large-scale clinical studies analyzing CCTA-derived metrics typically require ground-truth validation in the form of high-fidelity 3D intravascular imaging. However, manual rigid alignment of intravascular images to corresponding CCTA images is both time consuming and user-dependent. Moreover, intravascular modalities suffer from several non-rigid motion-induced distortions arising from distortions in the imaging catheter path. To address these issues, we here present a semi-automatic segmentation-based framework for both rigid and non-rigid matching of intravascular images to CCTA images. We formulate the problem in terms of finding the optimal *virtual catheter path* that samples the CCTA data to recapitulate the coronary artery morphology found in the intravascular image. We validate our co-registration framework on a cohort of $n = 40$ patients using bifurcation landmarks as ground truth for longitudinal and rotational registration. Our results indicate that our non-rigid registration significantly outperforms other co-registration approaches for luminal bifurcation alignment in both longitudinal (mean mismatch: 3.3 frames) and rotational directions (mean mismatch: 28.6 degrees). By providing a differentiable framework for automatic multi-modal intravascular data fusion, our developed co-registration modules

*Corresponding Author

significantly reduces the manual effort required to conduct large-scale multi-modal clinical studies while also providing a solid foundation for the development of machine learning-based co-registration approaches.

1 Introduction

Coronary computed tomography angiography (CCTA) is a three dimensional image modality that provides information on the presence, extent and severity of obstructive coronary artery disease (CAD) (Tzimas et al. [2022]). As such, CCTA allows for the detection of stenotic atherosclerotic sections and assists clinicians in diagnosing CAD and planning treatment. CCTA Images can also be used to create computational models of coronary blood flow, allowing for the non-invasive estimation of fractional flow reserve (FFR-CT); a key diagnostic parameter in assessing functional impairment (Uzu et al. [2019]).

Albeit widespread in use, CCTA provides primary information on *luminal* anatomy, with limited capacity in assessing soft-tissue intraplaque tissue components. CCTA also suffers from blooming artifacts in the presence of highly attenuating calcium deposits (Kim et al. [2015], Budoff et al. [2008]), which, combined with comparably low image resolution, creates difficulties in resolving highly calcified arteries. Multiple studies have also been conducted to quantify the degree to which CCTA can accurately assess CAD-related diagnostic metrics such as luminal area (Uzu et al. [2019]), calcium morphology (Takahashi et al. [2021]), and plaque burden (Fischer et al. [2013], De Graaf et al. [2013], Brodoefel et al. [2009]). The majority of such studies (Takahashi et al. [2021], Fischer et al. [2013], Uzu et al. [2019], Brodoefel et al. [2009]) validate the performance of CCTA by manually co-registering image slices taken along the CCTA artery to intravascular imaging modalities such as intravascular ultrasound (IVUS) and optical coherence tomography (OCT); both providing higher-fidelity visualization of the lumen and surrounding tissue. There is also an increasing interest in validating CCTA-derived segmentation algorithms against co-registered intravascular imaging frames, again necessitating such multimodal image assessment (Lin et al. [2021], van Assen et al. [2019]).

Manual co-registration of CCTA and intravascular images is, however, a challenging and time consuming task. Typically, cross-sectional frames of the artery of interest are extracted from the CCTA images which then have to be matched with corresponding frames from an intravascular acquisition through an imaging catheter pullback procedure. Rigid registration in the longitudinal and rotational directions is usually achieved by matching single landmarks in both modalities, such as a large bifurcation (Takahashi et al. [2021]). However, the beating of the heart, the irregular motion of the imaging catheter, and the rotation of the catheter about its own axis create non-rigid distortions that accumulate along the length of the pullback (Tsiknakis et al. [2021]). Manually correcting for such artifacts is prohibitively time-consuming, requiring a cardiologist to manually mark fiducial points in both images and shift images such that the annotated points sufficiently align (Carrier et al. [2014], Tu et al. [2011], Hebsgaard et al. [2015]). Although such techniques are accurate up to rigid translation, they require time investment from a trained expert to find matching features in both modalities, creating a need for computational algorithms that non-rigidly register CCTA images to corresponding intravascular data in an automatic fashion.

Automatic co-registration techniques typically consist of discretely optimizing a constructed cost function over a set of longitudinal or rotational image shifts, where the cost function varies depending on the modalities being registered. Some proposed cost functions include metrics such as lumen diameters (Qin et al. [2021]), lumen contours (Molony et al. [2016], Karmakar et al. [2020]), calcium thickness (Gharaibeh et al. [2020], Molony et al. [2016]), and image pixel intensities (Tsiknakis et al. [2021]). Similarly, rigid rotational registration for intravascular pullbacks has also been based on extracted features such as luminal contours (Karmakar et al. [2020]), and calcium angle (Molony et al. [2016]). However, the registration accuracy of all rigid registration methods is compromised by inconsistent motor pullback speeds and rotational drift, which introduce non-rigid longitudinal and rotational distortions that misalign image features such as diseased plaque and bifurcations.

To compensate for the longitudinal, rotational, and transverse motion of the catheter, several non-rigid registration approaches have been proposed, typically to be employed after initial rigid alignment. Currently, non-rigid registration of multiple intravascular imaging datasets has been predominantly performed through Dynamic Time Warping (DTW) and Dynamic Programming (DP) (Tsiknakis et al. [2021], Molony et al. [2016]). However, DTW introduces non-physiological assumptions into the registration process by discretely skipping or repeating intravascular frames, assumed to be evenly spaced along the longitudinal direction. As a result, DTW is not well suited for use for intravascular images, with pullback acquisitions sometimes rendering up to 10 repeated intravascular imaging frames at a time (Molony et al. [2016]). On the contrary, continuous non-rigid registration methods have been developed to model the longitudinal stretch and rotational drift between intravascular imaging frames using affine transforms and spline interpolation (Zhang et al. [2014], Uzu et al. [2019]). While such continuous non-rigid methods are more realistic, they extensively rely on manual annotations of all bifurcation zones for image registration, severely limiting their scalability. As such, there is

no continuous non-rigid registration method as of yet that does not explicitly require fiduciary landmarks for rotational and longitudinal alignment. Further, there has been an increasing interest in machine learning approaches to image co-registration in which a neural network is trained to predict a spatial transform that maps a moving image onto a static target image (Balakrishnan et al. [2019], Fu et al. [2020]). Such approaches critically rely on a differentiable and continuous spatial transform allowing for back-propagation of gradients to adjust the neural network weights (Jaderberg et al. [2015]). While such continuous and differential spatial transforms are available for co-registration of 3D and 2D medical images, a similar framework that accounts for the unique variation in intravascular catheter motion has not been developed.

Given the previous limitations noted in prior co-registration algorithms, we here propose a novel semi-automatic framework that takes as input an intravascular imaging pullback and a CCTA 3D image and aligns each intravascular image frame along the artery to the equivalent frame in the CCTA image. The proposed continuous registration methodology does not require manual matching of landmarks, with the only manual effort being the selection of viable intravascular imaging frames and the provision of a rough centerline within the CT image. Specifically, we explore the problem of reconstructing the path of a *virtual catheter* moving through and sampling from a 3D CCTA image such that the set of frames produced by the motion of the catheter optimally reflect the equivalent target intravascular pullback. Key contributions of this framework include:

- We present the first continuous co-registration framework for rigid and non-rigid matching of CCTA images and intravascular images up to pixelwise alignment, with segmentations of the lumen and vessel wall as sole input.
- We introduce a rigid registration approach that consists of our published longitudinal rigid registration algorithm, which uses lumen area in a multi-step decision process, and a rotational registration step that leverages the segmentation of the vessel wall to produce an initial rotational configuration for subsequent registration.
- We introduce a novel non-rigid registration step, based only on the lumen segmentation, which is robust to physiological catheter motions. The registration is formulated in terms of finding the path of a virtual catheter, which translates the CCTA image into an intravascular-like image by sampling the segmentation along the virtual catheter path. The virtual catheter path is reconstructed by spatially deforming the CCTA centerline by B-spline deformations formulated in the longitudinal, rotational, and transverse directions, ensuring a smooth and physiological reconstruction of catheter motion.
- Our non-rigid registration module being both continuous and differentiable, allows for easy integration into future machine-learning-based approaches for intravascular image registration.
- We validate in a direct clinical setting, evaluating performance across a multimodal cohort of cardiac patients ($n = 40$) and benchmarking performance against previously developed state-of-the-art approaches.

2 Methodology

An overview of the co-registration pipeline is detailed in Figure 1. In brief, bi-modality images are processed to produce binary segmentations of the lumen and vessel wall (section 2.1.1), which are first used in a rigid registration step, involving both longitudinal and rotational alignment (section 2.1.2). The rigid registration is then used as an initial estimate of a virtual catheter path forming the basis for a non-rigid registration (section 2.1.3). The virtual catheter path initially samples the geometry of the CT lumen to produce a virtual imaging pullback that is then compared to a Signed Distance Field (SDF) derived from the intravascular equivalent. A non-rigid transformation for the longitudinal, rotational, and transverse motion distortions is applied on the virtual catheter path and optimized to align the SDF's in both modalities. The performance of our proposed co-registration algorithm is then validated on a clinical cohort of relevant cardiac patients (section 2.2.2)

2.1 Co-registration framework

2.1.1 Preprocessing

As the basis for our co-registration pipeline, luminal segmentations from the two different image modalities are provided. Starting with the intravascular image set, luminal frame-by-frame segmentations are used to produce an SDF using a fast marching method (Treister and Haber [2016]), clamped to only have negative values (indicating that a pixel is inside the lumen). Further, the SDF is smoothed in the axial direction with a Gaussian convolutional kernel of size 3 and standard deviation 0.1 in order to regularize the optimization process.

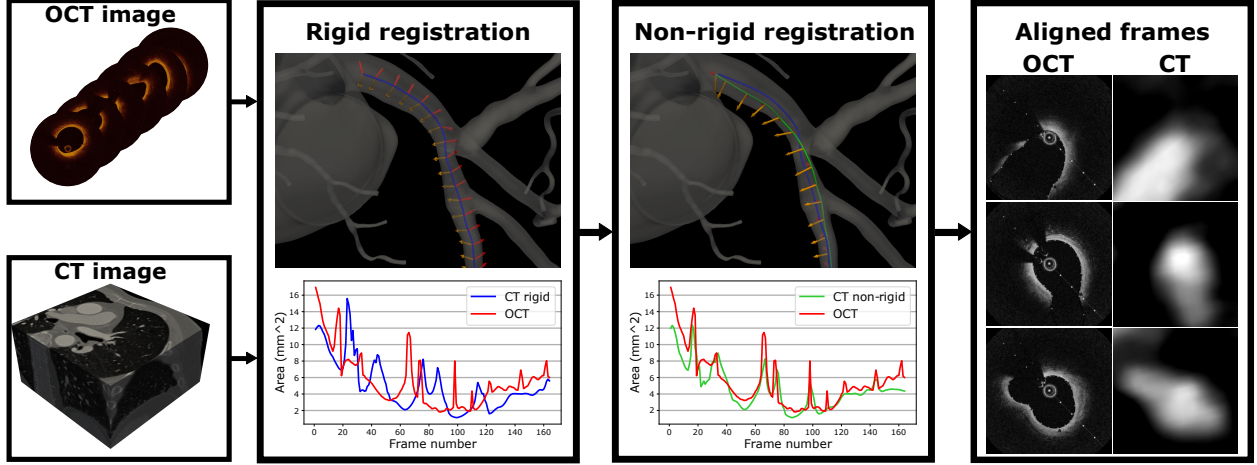


Figure 1: Overview of the proposed registration pipeline. The imaging modalities are rigidly co-registered in the longitudinal and rotational directions, serving as the basis for the initialization of the virtual pullback trajectory. The virtual pullback trajectory is then used to sample a CT lumen signed distance field (SDF), used in direct comparison to the equivalent OCT SDF.

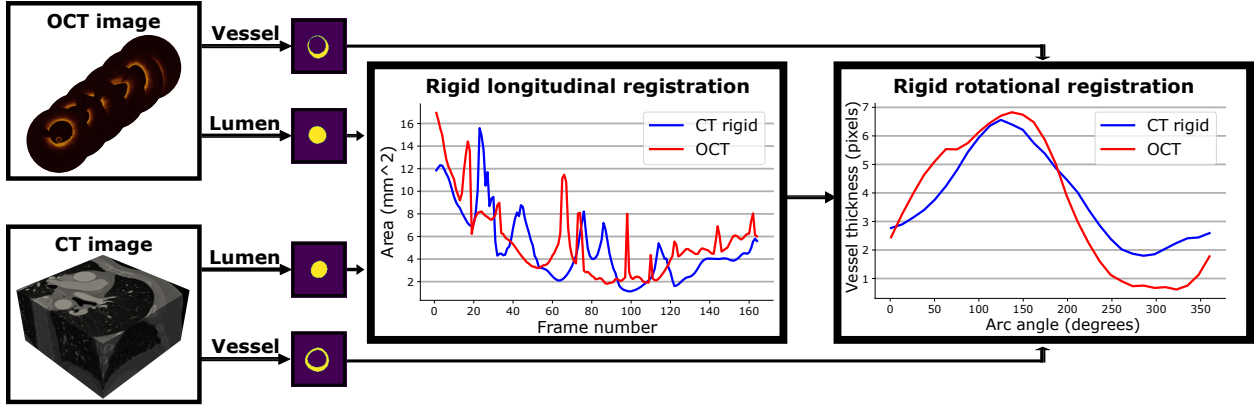


Figure 2: Overview of the proposed rigid registration pipeline. The lumen segmentation area vectors from both modalities are used to rigidly register the modalities in the longitudinal direction using a sliding window approach. The longitudinal registration is then used to match each equivalent frame for the rotational registration. The vessel wall segmentations are then converted to vessel thickness-arc angle plots and are used to determine an optimal rigid rotation.

Coupled to the intravascular image set, a corresponding 3D SDF from the CCTA images is generated. Although several methods could potentially be applied for such, a convenient approach is to derive the SDF from a computational mesh of the coronary tree. Herein, to create an SDF a narrow band is defined within the object mesh boundary, subsequently used to compute exact Euclidean distances from each voxel center to the boundary. Outside the object boundary, the distance field values are then set to zero. Corresponding binary segmentations can then be produced by simple thresholding operations. Using these computational meshes, vessel centerlines are obtained using VMTK (Antiga et al. [2008]), generating an array \bar{r} representing \mathbf{n} spatial positions with an axial spacing of 0.2mm. A spatial derivative is then applied to the centerline points \bar{r} , defining a tangent vector \mathbf{T} for each point. The two vectors \mathbf{U} and \mathbf{V} that are orthogonal to the tangent vector can then be obtained through the parallel transport method (Guo et al. [2013]), ensuring that the vectors \mathbf{V} and \mathbf{U} remain stable between frames placed along the axial direction. The centerline points and the orthogonal vectors hence define a set of frames $(\bar{r}, \mathbf{T}, \mathbf{U}, \text{and } \mathbf{V})$ in 3D space that are used to sample the CCTA SDF along an equivalent *virtual catheter* pullback, with dimensions equalling the intravascular dataset (in our case: $96 \times 96 \times N_{frames}$ with an in-plane resolution of 80 micrometers), all using a curved-planar reformation procedure (Kanitsar et al. [2002]). The resulting SDF is then smoothed in the axial direction with a Gaussian convolutional kernel of size 3 and standard deviation of 0.1. Through this method, virtual pullbacks of both the lumen and vessel segmentations were produced.

2.1.2 Rigid registration

An overview of the rigid registration step can be seen in Figure 2. For the rigid longitudinal registration, the processed lumen segmentations are used to create an area vector of equal lengths, sampling the CT virtual pullback to correspond to the acquired intravascular set. Here, We leverage our previous work to rigidly align the pullbacks using a multi-step sliding window method, minimizing the difference in area vectors (for details see (Karmakar et al. [2020])). Before registration, continuous segments of the OCT pullback with poor lumen segmentations due to residual blood or catheter housing were manually excluded.

For rigid rotational registration, the luminal profiles were deemed unreliable for producing good alignment. Therefore, the vessel border segmentations were instead used for rotationally aligning the pullbacks. For each CT and intravascular frame, respectively, a thickness-arc angle vector is extracted by tracing a set of radial rays from the centroid of the vessel segmentation in increments of 12 degrees. The thickness vectors are then matched according to the result of the longitudinal registration, with non-overlapping frames subsequently cropped. The optimal rigid rotation angle is then obtained by sliding the set of CT thickness vectors over each equivalent intravascular image vector and minimizing the mean squared error across all frames.

2.1.3 Non-rigid registration

The non-rigid registration process (Figure 3) consists of optimizing a set of frame variables (\bar{r} , \mathbf{T} , \mathbf{U} , and \mathbf{V}) representing a virtual catheter path moving through the CCTA image. The loss function to be optimized is defined as the mean squared error between the 3D SDF generated from the two image sets, with the CCTA-SDF sampled along the aforementioned virtual catheter path. The virtual pullback is initialized as the centerline that was calculated from the CCTA 3D model and longitudinally cropped and rotated according to the output of the rigid registration. After rigid registration a spline is defined based on the centerline points \bar{r} where the centerline points are fully described by their arclength values \bar{s} along the spline. Accordingly, every i -th frame can be manipulated by 4 variables, representing the arclength along the virtual catheter path s_i , the rotation angle of the frame θ_i about the catheter path \mathbf{T} , and the in-plane transverse displacements d_u and d_v along the frame vectors \mathbf{U} and \mathbf{V} respectively (see Figure 3).

To regularize the motion of the virtual catheter to be smooth and physiological, the 4 frame manipulation variable sets are parametrized by a sparse set of control points controlling a B-spline deformation (Rueckert et al. [1999]) independently acting on 4 nx1 vectors representing the frame manipulation variables \bar{s} , $\bar{\theta}$, \bar{d}_u , and \bar{d}_v . Thus, for a 1D control point grid of size N , the relation between a frame manipulation variable \mathbf{v} and the control points \mathbf{p} can be described by:

$$\mathbf{v}(s) = \sum_{i=0}^N \mathbf{B}_i(s) \mathbf{p}_i, \quad (1)$$

where $B_i(s)$ is a polynomial basis function of order 2. In matrix form, the same can be represented by:

$$\mathbf{V} = \mathbf{B}\mathbf{P}, \quad (2)$$

in which $\mathbf{V} \in \mathbb{R}^{n \times 1}$, $\mathbf{B} \in \mathbb{R}^{n \times N}$, $\mathbf{P} \in \mathbb{R}^{N \times 1}$ where n is the number of frames and N is the number of control points. B is the univariate B-spline tensor and can be pre-computed from the initial frame manipulation variable vectors, while \mathbf{P} is the deformed control point grid vector that is optimized during co-registration.

Instead of directly optimizing for the set of $N_s = 30$ control points P^s controlling the arclength variables s for each frame, the control point deformations ΔP_i^s can be parametrized by a deformation vector X^s of size $N_s - 1$. dictating the relative displacement of each control point from its proximal neighbor, with the most proximal control point being fixed. This is done to account for the cumulative effect of catheter motor speed variations on the rest of the pullback. Therefore, the deformation of each control point can be defined as the cumulative sum of the relative deformations along the proximal control points. Moreover, to regularize the catheter motion and prevent backwards movement, the relative deformation of each control point is limited to a fraction (0.35) of the distance between control points.

$$\Delta P_i^s = X_i^s + \sum_{j=0}^{i-1} X_j^s \quad (3)$$

Once the control points are deformed into a new configuration, the new arclength values for each frame \bar{s} is calculated through equation 2 and the frame vectors (\mathbf{T} , \mathbf{U} , and \mathbf{V}) are then recalculated.

$$\bar{s} = B^s P^s \quad (4)$$

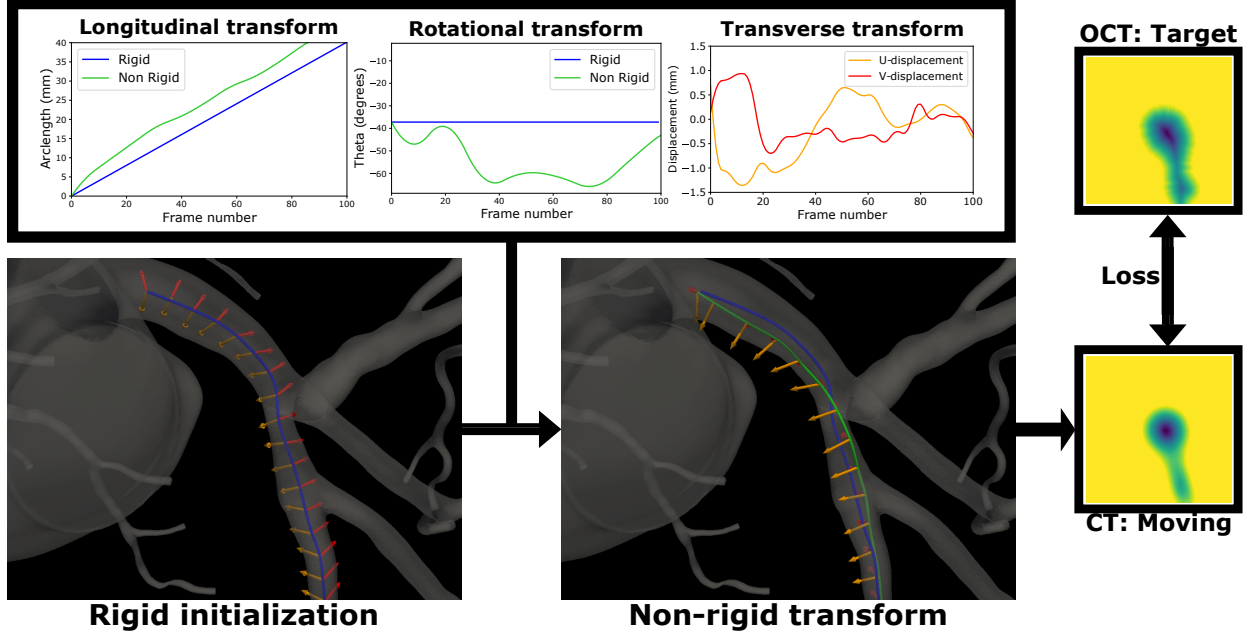


Figure 3: Overview of the spatial deformation acting on the virtual catheter path. The longitudinal transform stretches and compresses the space between adjacent frames, at which point the frame vectors (T , U , and V) are recalculated. The rotational transform is then applied to the frame vectors orthogonal to the tangent (U and V) about T , and the transverse transform is then applied to shift the centerline points in the direction of the new frame vectors (U and V).

2.1.4 Non-rigid rotational registration

Similar to the longitudinal registration, the set of $N_\theta = 20$ control points P^θ controlling the rotation of each frame about the catheter axis can be parameterized by a relative rotation vector X^θ of size N_θ . The rotation value for each control points is defined by:

$$\Delta P_i^\theta = X_i^\theta + \sum_{j=0}^{i-1} X_j^\theta \quad (5)$$

The rotation correction for each frame is applied after the non-rigid longitudinal transformation but before the non-rigid transverse transformation. Once the control points are deformed into a new configuration, the new rotation values for each frame $\bar{\theta}$ can be calculated through equation 2 and used to rotate frame vectors \mathbf{U} and \mathbf{V} about the tangent vectors \mathbf{T} .

$$\bar{\theta} = B^\theta P^\theta \quad (6)$$

2.1.5 Non-rigid transverse registration

The virtual catheter was biased to stay close to the centerline by optimizing the $N_d = 60$ control points determining the in-plane transverse displacements d_u and d_v directly. Thus the 2 orthogonal transverse displacements for each frame was calculated from the matrix relation:

$$\bar{d} = B^d P^d \quad (7)$$

Where for each frame the displacements along the vectors U and V were applied as a final step after the non-rigid longitudinal and rotational transforms.

2.2 Performance evaluation

2.2.1 Image data

To evaluate our proposed co-registration framework, a dataset consisting of $n = 40$ matched OCT and CT image pairs from 5 different clinical centers were selected, all originating from the Precise Percutaneous Coronary Intervention Plan (P3) study (Nagumo et al. [2021]). As each OCT pullback image consisted of 375 frames, the intravascular imaging dataset comprised of approximately 15,000 image frames. The OCT lumen in every frame was manually annotated by

trained cardiologists. Further, the vessel wall borders in every OCT frame were segmented using a convolutional neural network, using the previously published U-net as base architecture (Ronneberger et al. [2015]). Details of the network, training, and validation can be found in Supplementary Material A. The lumen and vessel wall segmentations were then re-sampled to represent a 3D image of dimensions $96 \times 96 \times N_{frames}$ with an in-frame resolution of 80 micrometers and an out-of-frame resolution of 0.4 mm. All utilized intravascular pullbacks were manually deemed as of sufficient image quality, with appropriate quality lumen segmentations. For the CCTA data, a 3D model of the coronary tree for each patient was produced by HeartFlow using the CCTA image (Sonck et al. [2022]). The 3D model was then used to produce a 3D SDF with a resolution of 0.25mm along each axis with an image dimension of $768 \times 768 \times 482$.

2.2.2 Co-registration accuracy

In order to evaluate the performance of the non-rigid registration, 114 bifurcations were manually marked in the OCT pullback as well as in the rigid and non-rigid virtual pullback segmentations generated from the CCTA data. Bifurcations were defined as the last image frame before a visual coronary artery split into two branches could be seen. Bifurcations that were common to both modalities had their frame numbers recorded for validation of the non-rigid registration algorithm. Longitudinal validation was conducted by comparing the frame number of a bifurcation in the OCT data with the equivalent bifurcation frame number in the virtual pullback before and after non-rigid registration. In order to validate the non-rigid rotational registration, the bifurcation angle difference between OCT pullback and the virtual pullback was compared before and after rotational registration. As the bifurcation angle between bifurcation sections that were not longitudinally matched is expected to be uncorrelated, a separate analysis was conducted to characterize how angular mismatch varies when the bifurcations are longitudinally matched. Furthermore, only bifurcations that had a frame mismatch below 6 frames were considered for extensive analysis of rotational accuracy.

2.2.3 Comparison to alternative approaches

The most common co-registration methodology employed for coronary artery registration has been discrete optimization approaches such as DTW and Dynamic Programming. Therefore, in order to evaluate the performance of our longitudinal and rotational co-registration framework against state-of-the-art discrete approaches, we applied the methodology described in Karmakar et. al (Karmakar et al. [2022]) on the same dataset used in this study. The approach utilizes DTW to longitudinally align two coronary imaging modalities and Dynamic Programming to rotationally align each frame. We utilized a window length of 4 (0.8mm) as implemented in the previous study and recorded identical alignment metrics for 114 matched bifurcations in the dataset. The non-rigid registration algorithm was applied after the rigid longitudinal registration step described in section 2.1.2. A substudy was also conducted in which the angular alignment of all bifurcations was compared to the angular alignment of longitudinally matched bifurcations.

2.2.4 Optimization details

The gradient descent-based optimization procedure was implemented in PyTorch with the Adam optimizer (Kingma and Ba [2014]). A learning rate of 0.001 was used for the non-rigid longitudinal parameters and a rate of 0.01 was used for both the rotational and transverse parameters. Each co-registration procedure was run for a minimum of 200 iterations to ensure convergence.

3 Results

3.1 Longitudinal Registration

Longitudinal registration plots in Figures 4 and 7A1-2 show that using rigid registration alone (Figure 7A1), few bifurcations were longitudinally aligned within 6 (dotted line), 4 (dashed line), or 2 (solid line) frame distances. However, after non-rigid alignment (Figure 7A2), distinct improvement can be observed with a majority of bifurcations are aligned within 6 frames. These results are visualized by the longitudinal mismatch plot (Figure 5A), revealing that after rigid alignment, the percentage of bifurcations matched within 2, 4, and 6 frames are 26.3, 42.1, and 57.9%, respectively, while after non-rigid alignment, these values increase to 60.5, 78.9, and 86.8%. Moreover, the scatterplot for non-rigid registration (A2) demonstrates that the majority of bifurcations (86% shown in green) were enhanced in terms of frame alignment, while a negligible number of bifurcations had slightly (11.4 % shown in orange) or significantly (2.6 % shown in red) worse alignment after non-rigid registration. Table 2 further demonstrates the effect of non-rigid registration, in which the mean frame difference after rigid registration was 7.9 frames and subsequently decreased to 3.3 frames after non-rigid registration.

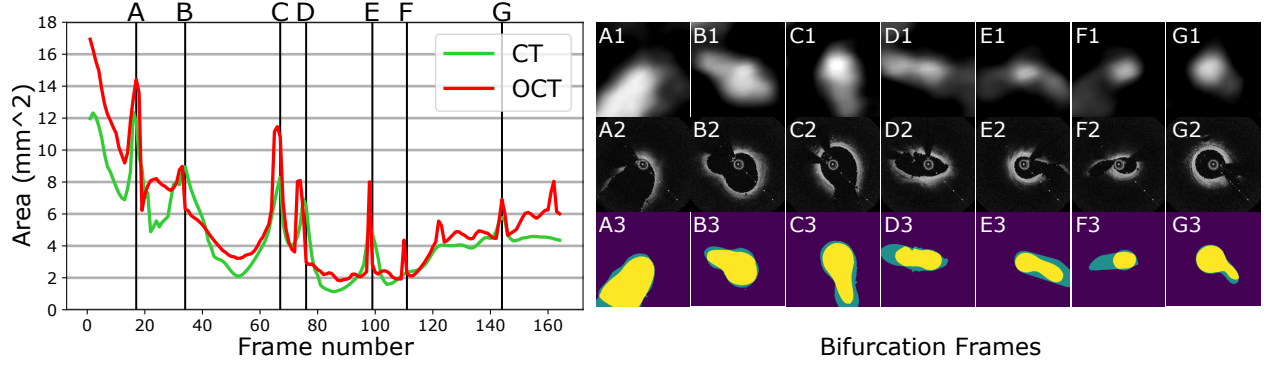


Figure 4: Qualitative results for a single co registered case. Top row shows area plot along the artery for the non-rigidly registered CT (green) and the OCT images. The bifurcation zones (Sections A-G) are marked and labeled for further analysis. Bifurcation frames from the CT, OCT, and overlapped segmentation maps are presented in the bottom row for qualitative analysis of the rotational and transverse co-registration.

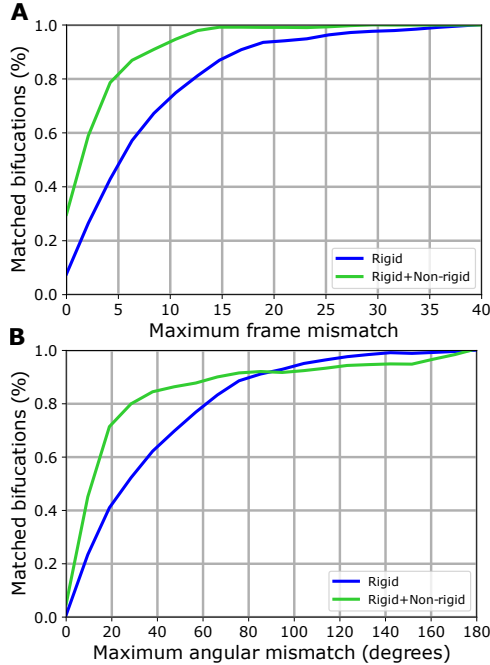


Figure 5: Quantitative results comparing the quality of rigid and non-rigid co registration in longitudinal and rotational directions with varying degrees of misalignment. The mismatch plots exhibit the % of matched bifurcations with increasing longitudinal (A) and rotational (B) alignment mismatch criteria (x-axis).

3.2 Rotational Registration

Examination of the individual bifurcating frames in figure 4 for the CT (row 1) and OCT (row 2) frames indicates excellent rotational and transverse alignment between both imaging modalities as evident from the raw images and the overlapped segmentations (row 3). Rotational registration plots in figure 7B1-2 demonstrate that few bifurcations are rotationally aligned within 30 (dotted line), 20 (dashed line), or 10 (solid line) degrees after rigid alignment (B1). After non-rigid alignment (Figure 7B2), a majority of bifurcations were aligned within 30 degrees, with a significant amount aligned within 20 and 10 degrees. Examination of the rotational mismatch plot (Figure 5B) quantitatively demonstrates an increase in the percentage of bifurcations aligned up to an angular mismatch of 10, 20, and 30 degrees from % values of 25.3, 40.4, and 52.3 to 51.5, 69.7, and 79.8% respectively. Similarly, the non-rigid registration scatterplot

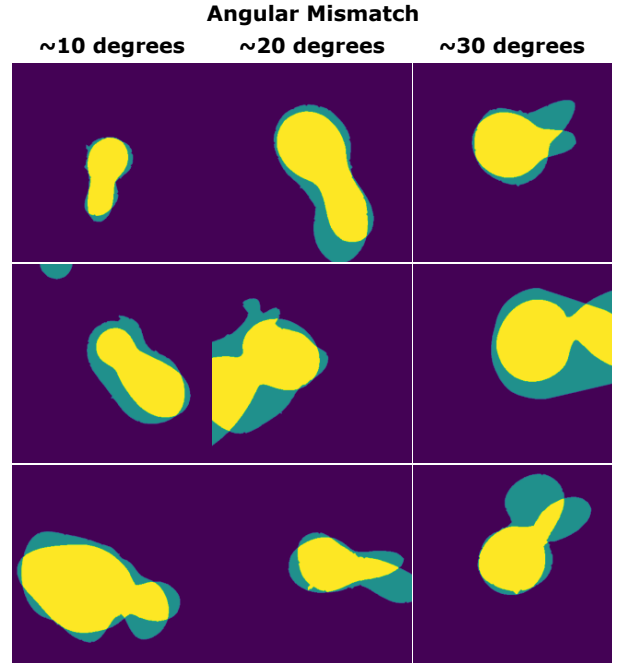


Figure 6: Grid plot showing multiple aligned bifurcation segmentations using an SDF-based loss. Angular mismatches up to 10, 20, and 30 degrees are shown in the first, second, and third columns respectively.

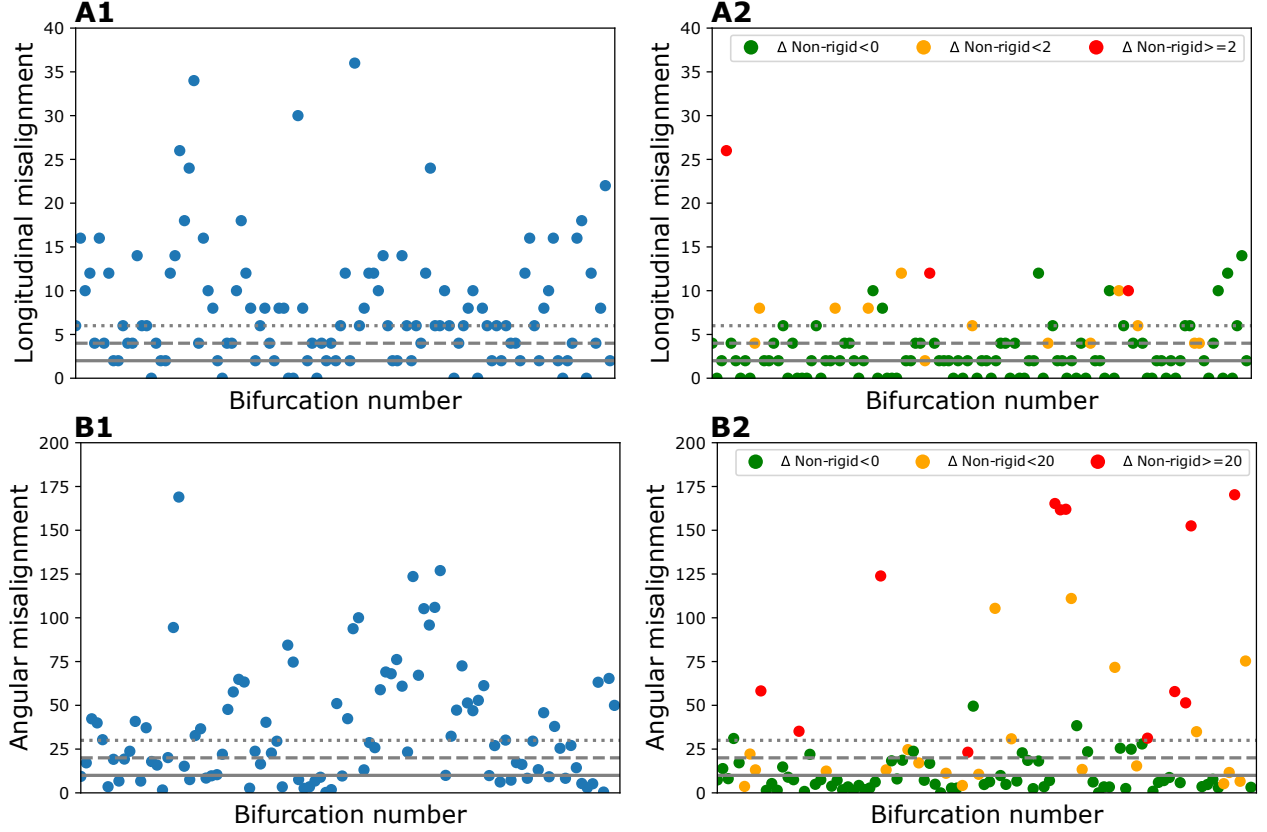


Figure 7: Quantitative results comparing the quality of rigid and non-rigid co-registration in longitudinal and rotational directions. The first row compares bifurcation frame mismatch before (A1) and after (A2) non-rigid registration in the form of scatterplots. The second row compares bifurcation angular mismatch before (B1) and after (B2) non-rigid registration in the form of scatterplots. The scatterplot for the longitudinal and rotational non-rigid registration (A2 and B2) are color-coded to exhibit the change in alignment metric after non-rigid registration, where green represents an increase in alignment, orange represents a mild decrease in alignment, and red represents a strong decrease in alignment. Only bifurcations that were longitudinally matched within 6 OCT frames were analyzed for rotational alignment.

demonstrates that the majority of bifurcations had their angular mismatch decreased after non-rigid alignment (66% shown in green) and only a minority had their angular mismatch values slightly (22% shown in orange) or significantly (12% shown in red) increased. The mean value of the angular mismatch before and after non-rigid alignment is reported in Table 2, in which the mean angular mismatch decreases from 36.0 to 28.6 degrees.

3.3 Comparison with previous approaches

A direct comparison of the virtual catheter method with state-of-the-art discrete optimization approaches can be seen in Tables 2 and 3. Comparing the virtual catheter method to a discrete optimization approach for longitudinal registration, it was shown that DTW produces significantly poorer results in longitudinal registration, with the longitudinal mismatch of 11.7 frames being higher than rigid longitudinal registration average of 7.9 frames. Comparing the virtual catheter method to using Dynamic Programming for rotational registration, it was shown that such discrete optimization algorithms exhibit poor performance for CT-OCT rotational registration (angular mismatch of 77.9 degrees) which is higher than the angular mismatch after rigid rotational registration alone. Table 3 quantifies the angular mismatch in the case where non-rigid longitudinal registration is successful. For bifurcations with a maximum frame mismatch of 6 after non-rigid registration, the angular mismatch decreases from 77.9 to 65.2 for the Dynamic Programming approach, while for the virtual catheter method, the angular mismatch decreases from 28.6 to 24.8. In contrast, the angular mismatch for the rigid registration is unchanged after excluding non-matching bifurcations.

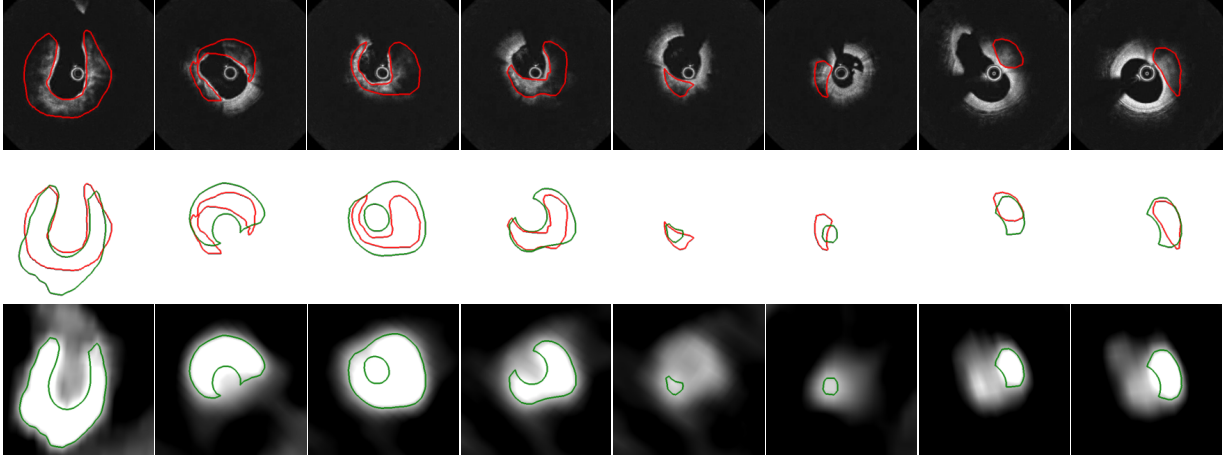


Figure 8: Qualitative results comparing the alignment of calcium annotations between OCT (first row) and CT (third row) for selected frames with good luminal alignment. The middle row shows the calcium annotations for OCT (red) and CT (green) superimposed on each other.

Table 1: Accuracy of alternative co-registration approaches, proposed for intravascular-intravascular image registration. Data is presented from left to right including evaluated co-registered modalities, dataset size, and overall methodological approach. Further, average errors are presented in both longitudinal (frames) and rotational (degree) directions.

| Ref. | Modalities | Dataset Size | Methodology | Longitudinal mismatch | Angular mismatch |
|-------------------------|------------|--------------|---------------------------|-----------------------|------------------|
| Karmakar et al. [2022] | OCT-OCT | 9 patients | DTW + Dynamic Programming | 0.9 ± 0.8 | 7.7 ± 6.7 |
| Tsiknakis et al. [2023] | OCT-OCT | 21 patients | DTW + Harmony Search | 5.6 ± 6.7 | 1.2 ± 0.81 |
| Karmakar et al. [2022] | OCT-IVUS | 7 patients | DTW + Dynamic Programming | 1.45 ± 0.7 | 29.1 ± 23.2 |
| Molony et al. [2016] | OCT-IVUS | 12 patients | DTW + Dynamic Programming | 5.0 ± 6.2 | 17.8 ± 21.9 |

Table 2: Accuracy of co-registration approaches applied to CT-OCT image registration. Data is presented from left to right including evaluated co-registered modalities, dataset size, and overall methodological approach. Further, average errors are presented in both longitudinal (frames) and rotational (degree) directions. All approaches in this table have been evaluated on the same dataset

| Ref. | Modalities | Dataset Size | Methodology | Longitudinal mismatch | Angular mismatch |
|------------------------|------------|--------------|---------------------------|-----------------------|------------------|
| Karmakar et al. [2022] | CT-OCT | 40 patients | DTW + Dynamic Programming | 11.7 ± 12.1 | 77.9 ± 61.0 |
| Ours (Rigid) | CT-OCT | 40 patients | Virtual Catheter Method | 7.9 ± 7.1 | 36.0 ± 31.9 |
| Ours (Rigid+Non-rigid) | CT-OCT | 40 patients | Virtual Catheter Method | 3.3 ± 3.9 | 28.6 ± 40.9 |

Table 3: Accuracy of co-registration approaches applied to CT-OCT image registration for bifurcations that are longitudinally matched. Data is presented from left to right including methodological approach and number of longitudinally matched bifurcations. Bifurcations are considered longitudinally matched when they have a maximum frame difference of 6 after non-rigid longitudinal registration. Further, average errors are presented for rotational direction in degrees.

| Ref. | Methodology | Matched Bifurcations | Angular Mismatch |
|------------------------|---------------------------|----------------------|------------------|
| Karmakar et al. [2022] | DTW + Dynamic Programming | 52/114 | 65.2 ± 72.9 |
| Ours (Rigid) | Virtual Catheter Method | 99/114 | 36.0 ± 33.0 |
| Ours (Rigid+Non-rigid) | Virtual Catheter Method | 99/114 | 24.8 ± 39.0 |

4 Discussion

The aim of the current study was to develop a fully automatic registration algorithm to align CCTA and intravascular images. Specifically, we propose a novel registration process finding the optimal rigid and non-rigid spatial transforms using a *virtual catheter* path in the CCTA data, aligning the non-invasive modality to its invasive counterpart. Our results indicate excellent co-registration accuracy, with excellent agreement with reference manual landmark annotations (Figure 4). Further, our results underline the critical importance of a non-rigid registration step, with significant enhancement in both longitudinal and rotational alignments observed when comparing rigid vs. non-rigid alignments in Table 2. We demonstrate that for the vast majority of bifurcations, our framework is able to improve the longitudinal and rotational alignment of common bifurcations within the CT and OCT images. Lastly, we demonstrate the added value of our approach as compared to state-of-the-art alternatives, with a head-to-head comparison to previously developed discrete optimization alignment algorithms (Table 1). A head-to-head comparison demonstrates that discrete optimization approaches for longitudinal and rotational alignment suffer a significant drop in alignment quality when applied for the task of CT-OCT co-registration. Meanwhile, our approach maintains performance accuracy in line with simpler tasks such as intravascular-intravascular image registration.

4.1 Related work

Currently, a majority of CCTA studies that validate their CT findings with intravascular images have used rigid manual registration based on fiducial landmarks such as bifurcations or large calcifications (Carlier et al. [2014], Tu et al. [2011], Hebsgaard et al. [2015]). One of the few studies that attempted to align CT and intravascular data up to a non-rigid level is by Uzu et al. [2019] in which a B-spline deformation model was used to optimize the alignment of manually annotated bifurcation landmarks. Though powerful, such an approach is time-consuming due to the significant amount of manual processing required to process the OCT images, rigidly align the geometric models, and mark bifurcations within every artery. In comparison, our approach implicitly matches nearby bifurcations using longitudinally smoothed SDFs representing the CT and OCT lumens, respectively. Other approaches that register intravascular-to-intravascular modalities have in the past relied on DTW (Molony et al. [2016], Karmakar et al. [2022]), discretely optimizing the frame-wise progression of one intravascular pullback to maximize longitudinal and rotational alignment with another. Such methods, nevertheless, attempt to recapitulate the continuous motion distortions introduced by the catheter path with discrete non-physiological frames or repeats (Molony et al. [2016]). However, skipping or repeating several frames that the catheter motion is not smooth or continuous, which is an unrealistic assumption about the catheter path.

Direct numerical comparison of reported co-registration accuracy across published approaches is inherently difficult as co-registration accuracy is highly dependent on the specific dataset explored as well as which modalities are being coregistered. For example, the simplest co-registration task would be represented by the alignment of same-modality images such as OCT-OCT image pairs. For such tasks, our previously published DTW and dynamic programming approach (Karmakar et al. [2022]) exhibits similar performance compared to other state-of-the-art algorithms (Tsiknakis et al. [2023]) (See Table 1). When applied to multimodality datasets, such as IVUS-OCT image pairs, our previously developed approach (Karmakar et al. [2022]) suffers distinctive drops in both longitudinal and rotational accuracy (see Table 1), however, still maintains comparative performance to similar Dynamic Programming approaches (Molony et al. [2016]). Thus, in order to facilitate a head-to-head comparison on the more challenging task of registering CT-OCT image pairs, we applied our previously developed discrete optimization algorithm (Karmakar et al. [2022]) on our multi-modal dataset of 40 patients. Doing so, we found that our previous approach produced significantly worse longitudinal and rotational alignment compared to the virtual catheter method, with both longitudinal and angular alignment being worse than simple rigid registration (Table 2). In contrast, our developed methodology achieves competitive results with even intravascular-intravascular registration studies (Table 1 and Table 2).

4.2 Methodological Adaptations

From the above it can be seen that the task of co-registering CT and OCT images presents several unique difficulties for discrete registration algorithms. Our framework has several features that were designed to mitigate such challenges. First, the low resolution of CT images induces a circular bias in the lumen segmentations (see Figure 4), as well as a tendency to miss small bifurcations. Such circularly symmetric regions hence create zones of longitudinal and rotational ambiguity along the pullback. Our approach tries to minimize the dependency of such by formulating the longitudinal and rotational transforms acting on the virtual path in terms of a regularized and smooth B spline deformation. As such, the optimization procedure is mainly dominated by the alignment of prominent non-symmetric features such as bifurcations, rather than the circularly symmetric lumen segments. This ensures that the rotational alignment of all non-bifurcating lumen frames that are in proximity to matched bifurcations are properly matched due to B spline interpolation (Figure 4). Another significant issue faced in previous rotational co-registration algorithms (Karmakar

et al. [2022], Molony et al. [2016]) is that lumen bifurcations are only able to contribute to rotational alignment if they exist within the same frame. As such, poor longitudinal alignment of bifurcations was a significant contributing factor to the poor performance of our previously developed dynamic programming algorithm for rotational co-registration (Table 2). Our framework, in contrast, minimizes this dependency through the use of a Gaussian smoothing kernel applied longitudinally over the SDF. Longitudinal smoothing allows single-frame bifurcations to appear in adjacent frames and smooths the loss surface such that bifurcations in the different modalities can be better aligned (Figures 4 and 7). Another design choice that was found to increase training stability and co-registration quality was the use of SDF’s to determine alignment, as opposed to using a segmentation loss such as cross-entropy or Dice. This was due to the fact that when the lumen segmentations were fully overlapping, multiple rotational and transverse configurations contribute equally to a segmentation loss function, preventing the algorithm from making fine adjustments in the spatial transform. Figure 6 further demonstrates how the quality of rotational registration varies with angular mismatch, where the angular mismatch tends to occur due to the limitations of local optimization of pixel alignment. At less than 10 degrees mismatch, the difference in alignment is minimal, while under 30 degrees, the difference in alignment can be attributed to differing lumen bifurcation shapes in the CT and OCT data. Lastly, many co-registration methods normalize the position of the lumen by the artery centroid (Uzu et al. [2019], Karmakar et al. [2020, 2022], Molony et al. [2016]). While such an approach manages to align CT and OCT frames with circularly symmetric lumen, it fails to effectively align equivalent frames with bifurcations as the segmentation can have different maximum diameters between the modalities and thus different centroids. Moreover, centering the image around the lumen centroids can cause the algorithm to align bifurcations 180-degrees from the correct orientation. It was empirically found that this phenomenon was found to be a significant contributing factor to the degradation of the co-registration performance of our previously developed discrete co-registration algorithm. In this framework, we instead choose to jointly optimize for the transverse displacements of the virtual path in addition to the longitudinal and rotational displacements, which allows for the bifurcations in both modalities to be anchored around the OCT catheter location and enables near pixelwise alignment of the lumen (Figures 4,6) and plaque constituents such as calcium (Figure 8).

4.3 Limitations

Though very promising for clinical applications, our developed approach has a number of limitations. First, the non-rigid spatial transform acting on the virtual catheter path is found through gradient-based optimization, requiring that landmarks lie sufficiently close such that proper matching is ensured. For example, common bifurcations that have a frame mismatch of more than 6 frames (corresponding to the longitudinal smoothing kernel) are expected to be uncorrelated in terms of orientation. This issue can be mitigated by integrating deep learning networks which can accurately predict the spatial transform needed to align the two modalities. Another limitation is the dependence of non-rigid registration on the lumen. The lumen estimation is expected to be accurate for both modalities and as such, ensures good registration accuracy for regions that include many bifurcations. However, due to the poor resolution of CCTA images, the lumen estimation tends to be highly circular. Accordingly, it is expected that rotational co-registration certainty increases with bifurcation proximity but decreases in stenotic regions that contain highly circular CT luminal profiles. In the future, co-registration accuracy can likely be improved by including contextual information relating to the vessel wall such as lesion content and morphology as a supervisory signal in the loss function. Third, the use of a pixel-wise loss as a surrogate for luminal alignment may not necessarily result in optimal alignment of lumen bifurcations. As seen in Figure 6, a pixel-wise loss function can occasionally bias the spatial transform to align the central lumen body over aligning the bifurcation in scenarios where the bifurcation shapes are not perfectly matching. In the future, this issue can be mitigated by introducing an orientation loss to bias the spatial transform to rotationally align bifurcations. Lastly, regularizing the spatial transform and smoothing the SDF’s can create difficulties in localizing landmarks up to frame-wise precision. This can be seen in the area curve in Figure 4 section B with the slightly mismatched bifurcation and in Figure 7 A2 and B2 with a minor amount of bifurcations with increased frame and angular mismatch values. The localization capabilities of the algorithm can be improved by introducing multi-scale deformation steps where finer control point grids can be recursively used as the basis for the spatial transform.

4.4 Translational Benefits

The development of automatic frame-wise matching algorithms for CT-OCT data fusion would enable the development of several research-based applications. First, intravascular imaging data can act as ground truth to validate the reliability of CT in delineating several morphological metrics of atherosclerosis, such as luminal area, lipid content, and calcium volume. Understanding when CT-derived morphological metrics are reliable is critical for both therapy planning and deciding when to rely on intravascular imaging. For example, studying the interaction between calcium blooming and measured lumen size in CT images necessitates that ground truth lumen measurements be available, which can only be provided by frame-wise co-registration algorithms. Figure 8 demonstrates that such a frame-by-frame comparison can be done provided that longitudinal and rotational co-registration is of sufficient quality. Second, multi-modal data fusion

would allow for the enhanced generation of patient-specific digital twins from coronary images. There has been an increasing interest in the use of intravascular-images to create computational digital twins for the prediction of coronary pathophysiology and clinical decision-making (Kadry et al. [2021]). However, intravascular images, while providing excellent resolution within the imaging frame, do not provide sufficient information to create a fully physiological artery model. Intravascular images typically suffer from intra-frame motion drift artifacts in the longitudinal and rotational directions and cannot capture information on the three-dimensional centerline of the artery. On the other hand, CT suffers from poor resolution but is able to capture the three-dimensional nature of the artery with high accuracy. Combining both modalities would allow researchers to investigate the importance of longitudinal and rotational distortions, as well as modeling arterial tortuosity.

References

- Georgios Tzimas, Gaurav S Gulsin, Hidenobu Takagi, Niya Mileva, Jeroen Sonck, Olivier Muller, Jonathon A Leipsic, and Carlos Collet. Coronary ct angiography to guide percutaneous coronary intervention. *Radiology: Cardiothoracic Imaging*, 4(1):e210171, 2022.
- Kenzo Uzu, Hiromasa Otake, Gilwoo Choi, Takayoshi Toba, Hyun Jin Kim, Arjun Roy, Michiel Schaap, Leo Grady, Masahito Kawata, Toshiro Shinke, et al. Lumen boundaries extracted from coronary computed tomography angiography on computed fractional flow reserve (ffrct): validation with optical coherence tomography. *Eurointervention: Journal of Europcr in Collaboration with the Working Group on Interventional Cardiology of the European Society of Cardiology*, 14(15):e1609–e1618, 2019.
- Choongki Kim, Sung-Jin Hong, Dong-Ho Shin, Jung-Sun Kim, Byeong-Keuk Kim, Young-Guk Ko, Donghoon Choi, Yangsoo Jang, and Myeong-Ki Hong. Limitations of coronary computed tomographic angiography for delineating the lumen and vessel contours of coronary arteries in patients with stable angina. *European Heart Journal-Cardiovascular Imaging*, 16(12):1358–1365, 2015.
- Matthew J Budoff, David Dowe, James G Jollis, Michael Gitter, John Sutherland, Edward Halamert, Markus Scherer, Raye Bellinger, Arthur Martin, Robert Benton, et al. Diagnostic performance of 64-multidetector row coronary computed tomographic angiography for evaluation of coronary artery stenosis in individuals without known coronary artery disease: results from the prospective multicenter accuracy (assessment by coronary computed tomographic angiography of individuals undergoing invasive coronary angiography) trial. *Journal of the American College of Cardiology*, 52(21):1724–1732, 2008.
- Yu Takahashi, Takayoshi Toba, Hiromasa Otake, Yusuke Fukuyama, Shinsuke Nakano, Yoichiro Matsuoka, Kosuke Tanimura, Yu Izawa, Hiroyuki Kawamori, Atsushi K Kono, et al. Feasibility of morphological assessment of coronary artery calcification with electrocardiography-gated non-contrast computed tomography: a comparative study with optical coherence tomography. *The International Journal of Cardiovascular Imaging*, 37(4):1445–1453, 2021.
- Collin Fischer, Edward Hulten, Pallavi Belur, Ryan Smith, Szilard Voros, and Todd C Villines. Coronary ct angiography versus intravascular ultrasound for estimation of coronary stenosis and atherosclerotic plaque burden: a meta-analysis. *Journal of cardiovascular computed tomography*, 7(4):256–266, 2013.
- Michiel A De Graaf, Alexander Broersen, Pieter H Kitslaar, Cornelis J Roos, Jouke Dijkstra, Boudewijn PF Lelieveldt, J Wouter Jukema, Martin J Schali, Victoria Delgado, Jeroen J Bax, et al. Automatic quantification and characterization of coronary atherosclerosis with computed tomography coronary angiography: cross-correlation with intravascular ultrasound virtual histology. *The international journal of cardiovascular imaging*, 29(5):1177–1190, 2013.
- H Brodoefel, C Burgstahler, M Heuschmid, A Reimann, F Khosa, A Kopp, S Schroeder, CD Claussen, and ME Clouse. Accuracy of dual-source ct in the characterisation of non-calcified plaque: use of a colour-coded analysis compared with virtual histology intravascular ultrasound. *The British journal of radiology*, 82(982):805–812, 2009.
- A Lin, N Manral, P McElhinney, A Killekar, H Matsumoto, S Cadet, S Achenbach, SJ Nicholls, DT Wong, D Berman, et al. Deep learning-based plaque quantification from coronary computed tomography angiography: external validation and comparison with intravascular ultrasound. *European Heart Journal*, 42(Supplement_1):ehab724–0161, 2021.
- Marly van Assen, Akos Varga-Szemes, U Joseph Schoepf, Taylor M Duguay, H Todd Hudson, Svetlana Egorova, Kjell Johnson, Samantha St Pierre, Beatrice Zaki, Matthijs Oudkerk, et al. Automated plaque analysis for the prognostication of major adverse cardiac events. *European Journal of Radiology*, 116:76–83, 2019.
- Nikos Tsiknakis, Constantinos Spanakis, Panagiota Tsompou, Georgia Karanasiou, Gianna Karanasiou, Antonis Sakellarios, George Rigas, Savvas Kyriakidis, Michael Papafaklis, Sotirios Nikopoulos, et al. Ivus longitudinal and axial registration for atherosclerosis progression evaluation. *Diagnostics*, 11(8):1513, 2021.

- Stéphane Carlier, Rich Didday, Tristan Slots, Peter Kayaert, Jeroen Sonck, Mike El-Mourad, Nicolas Preumont, Dany Schoors, and Guy Van Camp. A new method for real-time co-registration of 3d coronary angiography and intravascular ultrasound or optical coherence tomography. *Cardiovascular Revascularization Medicine*, 15(4): 226–232, 2014.
- Shengxian Tu, Niels R Holm, Gerhard Koning, Zheng Huang, and Johan HC Reiber. Fusion of 3d qca and ivus/oct. *The international journal of cardiovascular imaging*, 27(2):197–207, 2011.
- Lasse Hebsgaard, Troels Munck Nielsen, Shengxian Tu, Lars Romer Krusell, Michael Maeng, Karsten Tange Veien, Bent Raungaard, Christian Juhl Terkelsen, Anne Kaltoft, Johan HC Reiber, et al. Co-registration of optical coherence tomography and x-ray angiography in percutaneous coronary intervention. the does optical coherence tomography optimize revascularization (doctor) fusion study. *International journal of cardiology*, 182:272–278, 2015.
- Hui Qin, Chunming Li, Yingguang Li, Jiayue Huang, Fan Yang, Takashi Kubo, Takashi Akasaka, Changyan Xiao, Juan Luis Gutiérrez-Chico, and Shengxian Tu. Automatic coregistration between coronary angiography and intravascular optical coherence tomography: Feasibility and accuracy. *JACC: Asia*, 1(2):274–278, 2021.
- David S Molony, Lucas H Timmins, Emad Rasoul-Arzrumly, Habib Samady, and Don P Giddens. Evaluation of a framework for the co-registration of intravascular ultrasound and optical coherence tomography coronary artery pullbacks. *Journal of biomechanics*, 49(16):4048–4056, 2016.
- Abhishek Karmakar, Max L Olender, Farhad Rikhtegar Nezami, David Marlevi, Evan Shlofmitz, Richard A Shlofmitz, and Elazer R Edelman. Detailed investigation of lumen-based tomographic co-registration. In *2020 IEEE International Conference on Bioinformatics and Biomedicine (BIBM)*, pages 1038–1042. IEEE, 2020.
- Yazan Gharaibeh, Juhwan Lee, David Prabhu, Pengfei Dong, Vladislav N Zimin, Luis A Dallan, Hiram Bezerra, Linxia Gu, and David Wilson. Co-registration of pre-and post-stent intravascular oct images for validation of finite element model simulation of stent expansion. In *Medical Imaging 2020: Biomedical Applications in Molecular, Structural, and Functional Imaging*, volume 11317, pages 306–316. SPIE, 2020.
- Ling Zhang, Richard Downe, Zhi Chen, Shanhui Sun, T Masiarov, Tomas Kovarnik, John Lopez, Milan Sonka, and Andreas Wahle. Side-branch guided registration of intravascular ultrasound pullbacks in coronary arteries. In *MICCAI Workshop in Computing and Visualization for IntraVascular Imaging and Computer Assisted Stenting (CVII-STENT)*, pages 44–51, 2014.
- Guha Balakrishnan, Amy Zhao, Mert R Sabuncu, John Guttag, and Adrian V Dalca. Voxelmorph: a learning framework for deformable medical image registration. *IEEE transactions on medical imaging*, 38(8):1788–1800, 2019.
- Yabo Fu, Yang Lei, Tonghe Wang, Walter J Curran, Tian Liu, and Xiaofeng Yang. Deep learning in medical image registration: a review. *Physics in Medicine & Biology*, 65(20):20TR01, 2020.
- Max Jaderberg, Karen Simonyan, Andrew Zisserman, et al. Spatial transformer networks. *Advances in neural information processing systems*, 28, 2015.
- Eran Treister and Eldad Haber. A fast marching algorithm for the factored eikonal equation. *Journal of Computational physics*, 324:210–225, 2016.
- Luca Antiga, Marina Piccinelli, Lorenzo Botti, Bogdan Ene-Iordache, Andrea Remuzzi, and David A Steinman. An image-based modeling framework for patient-specific computational hemodynamics. *Medical & biological engineering & computing*, 46(11):1097–1112, 2008.
- Jixiang Guo, Shun Li, Yim Pan Chui, Jing Qin, and Pheng Ann Heng. Mesh quality oriented 3d geometric vascular modeling based on parallel transport frame. *Computers in Biology and Medicine*, 43(7):879–888, 2013.
- Armin Kanitsar, Dominik Fleischmann, Rainer Wegenkittl, Petr Felkel, and Eduard Groller. *CPR-curved planar reformation*. IEEE, 2002.
- Daniel Rueckert, Luke I Sonoda, Carmel Hayes, Derek LG Hill, Martin O Leach, and David J Hawkes. Nonrigid registration using free-form deformations: application to breast mr images. *IEEE transactions on medical imaging*, 18(8):712–721, 1999.
- Sakura Nagumo, Carlos Collet, Bjarne L Norgaard, Hiromasa Otake, Brian Ko, Bon-kwon Koo, Jonathon Leipsic, Daniele Andreini, Ward Heggermont, Jesper M Jensen, et al. Rationale and design of the precise percutaneous coronary intervention plan (p3) study: Prospective evaluation of a virtual computed tomography-based percutaneous intervention planner. *Clinical cardiology*, 44(4):446–454, 2021.
- Olaf Ronneberger, Philipp Fischer, and Thomas Brox. U-net: Convolutional networks for biomedical image segmentation. In *International Conference on Medical image computing and computer-assisted intervention*, pages 234–241. Springer, 2015.

- Jeroen Sonck, Sakura Nagumo, Bjarne L Norgaard, Hiromasa Otake, Brian Ko, Jinlong Zhang, Takuya Mizukami, Michael Maeng, Daniele Andreini, Yu Takahashi, et al. Clinical validation of a virtual planner for coronary interventions based on coronary ct angiography. *Cardiovascular Imaging*, 15(7):1242–1255, 2022.
- Abhishek Karmakar, Max L Olender, David Marlevi, Evan Shlofmitz, Richard A Shlofmitz, Elazer R Edelman, and Farhad R Nezami. Framework for lumen-based nonrigid tomographic coregistration of intravascular images. *Journal of Medical Imaging*, 9(4):044006, 2022.
- Diederik P Kingma and Jimmy Ba. Adam: A method for stochastic optimization. *arXiv preprint arXiv:1412.6980*, 2014.
- Nikos Tsiknakis, Constantinos Spanakis, Panagiota Tsoumpou, Georgia Karanasiou, Gianna Karanasiou, Antonis Sakellarios, George Rigas, Savvas Kyriakidis, Michail I Papafaklis, Sotirios Nikopoulos, et al. Oct sequence registration before and after percutaneous coronary intervention (stent implantation). *Biomedical Signal Processing and Control*, 79:104251, 2023.
- Karim Kadry, Max L Olender, David Marlevi, Elazer R Edelman, and Farhad R Nezami. A platform for high-fidelity patient-specific structural modelling of atherosclerotic arteries: from intravascular imaging to three-dimensional stress distributions. *Journal of the Royal Society Interface*, 18(182):20210436, 2021.